https://doi.org/10.5194/acp-2020-1128
Preprint. Discussion started: 2 December 2020

Atmospheric Chemistry and Physics
Discussions
Open Access
EGU

Analysis of CO_2 spatiotemporal variations in China using tower data and a weather-biosphere-online-coupled model, WRF-VPRM

Xinyi Dong[1,2], Man Yue[1,2], Yujun Jiang[3,4], Xiao-Ming Hu[5], Qianli Ma[4], Jingjiao Pu[3], and Guangqiang Zhou[6]

[1]School of Atmospheric Science, Nanjing University, Nanjing, 210023, China
[2]Joint International Research Laboratory of Atmospheric and Earth System Sciences & Institute for Climate and Global Change Research, Nanjing University, Nanjing, 210023, China
[3]Zhejiang Meteorological Science Institute, Hangzhou 310008, China
[4]Zhejiang Lin'an Atmospheric Background National Observation and Research Station, Hangzhou 311307, China
[5]Center for Analysis and Prediction of Storms, University of Oklahoma, Norman, Oklahoma, 73072, USA
[6]Shanghai Key Laboratory of Health and Meteorology, Shanghai Meteorological Service, Shanghai, 200135, China

Correspondence to: Yujun Jiang (yjjiang@pku.org.cn) and Xiao-Ming Hu (xhu@ou.edu)

Abstract. Dynamics of CO_2 has received considerable attention in the literature, yet significant uncertainties remain within the estimates of contribution from terrestrial flux and the influence of atmospheric mixing. In this study we apply the Weather Research and Forecasting model coupled with Vegetation Photosynthesis and Respiration Model (WRF-VPRM) in China to characterize CO_2 dynamics with tower data collected at a background site Lin'an (30.30˚N, 119.75˚E). The online coupled weather-biosphere WRF-VPRM simulations are able to simulate biosphere processes (photosynthetic uptake and ecosystem respiration) and meteorology in one coordinate system. Simulations are conducted for three years (2016-2018) with fine grid resolution (20 km) to detail the spatiotemporal variations of CO_2 fluxes and concentrations. This is the first attempt to apply the weather-biosphere model for a multi-year simulation with integrated data from a satellite product, flask samplings, and tower measurements to diagnose the dynamics of CO_2 in China. We find that the spatial distribution of CO_2 is determined by anthropogenic emissions, while its seasonality (with maximum concentrations in April 15 ppmv higher than minimums in August) is dominated by terrestrial flux and background CO_2. Observations and simulations reveal a consistent increasing trend in column-averaged CO_2 (XCO_2) of 0.6%/yr resulting from anthropogenic emission growth and biosphere uptake. WRF-VPRM successfully reproduces ground-based measurements of surface CO_2 concentration with mean bias of -0.79 ppmv (-0.20%) and satellite derived XCO_2 with mean bias of 0.76 ppmv (0.19%). The model-simulated seasonality is also consistent with observations, with correlation coefficients of 0.90 and 0.89 for ground-based measurements and Orbiting Carbon Observatory-2 (OCO-2) satellite data, respectively. However, evaluation against Lin'an tower data reveals uncertainty within the model for simulating the intensity and diurnal variation of terrestrial flux, which contributes to overestimation by ~5.35 ppmv (1.26%). Lin'an tower observations also reveal a strong correlation (-0.85) between vertical CO_2 and temperature

https://doi.org/10.5194/acp-2020-1128
Preprint. Discussion started: 2 December 2020

gradients, suggesting a significant influence of boundary layer thermal structure on the accumulation and depletion of atmospheric CO_2.

1 Introduction

Climate research requires accurate characterization of atmospheric CO_2, which is closely affected by the both atmospheric transport and terrestrial sources and sinks (Bauska et al., 2015; Keenan et al., 2016). Our current knowledge largely comes from interpreting ground- or space-based measurements and model simulations. While observation is limited by spatial and temporal coverages, modelling approaches also suffer from various uncertainties (Shi et al., 2018). Modelling assessment of CO_2 is usually conducted through two methods: first, process- or data-driven biosphere models in which terrestrial fluxes are diagnostically calculated with theoretical functions (Tian et al., 2015) or determined through semi-empirical relationships derived from ground measurements and/or satellite products with machine learning techniques (Papale and Valentini, 2003); second, inverse modelling in which prior flux estimates applied in atmospheric transport models are calibrated by observational data and/or satellite products to determine posterior terrestrial flux (Peylin et al., 2002). Process-driven biosphere models have difficulties capturing spatial and temporal variabilities at fine resolution because parameters calibrated from a limited number of site observations are applied across a variety of land covers (Todd-Brown et al., 2013). Atmospheric inverse modelling is predominantly affected by the presumed prior flux, and different assimilation techniques can give different and even conflicting results (Peylin et al., 2013). These fundamental features highlight the limits of these approaches for accurately modelling carbon dynamics.

Researchers have attempted to reconcile differences between "bottom-up" biosphere models and "top-down" atmospheric inverse models, and recent studies have demonstrated increasing levels of agreement owing to improved understanding of both approaches, such as better parameterization of biosphere processes (Dayalu et al., 2018), more accurately constrained estimates of prior flux (Crowell et al., 2018;Feng et al., 2019), and advanced measurement/satellite instruments that provide high quality data for assimilation (Gaubert et al., 2019); however, critical model disagreements still persist (Kondo et al., 2020). To bridge the gap between terrestrial flux and atmospheric mixing, a type of weather-biosphere coupled model (Ahmadov et al., 2007;Mahadevan et al., 2008) was developed to simulate biosphere processes and meteorology conditions in one coordinate system, allowing their interactions to be properly addressed. A few case studies (Ahmadov et al., 2009;Kretschmer et al., 2012;Park et al., 2018) have demonstrated the potential advantages of coupled weather-biosphere models over pure biosphere/inverse models for short term (a few weeks) simulations, but whether the coupled model is able to reproduce the spatial distributions and temporal variations and subsequently estimate carbon fluxes at regional scales with high confidence remains a crucial issue to be addressed.

https://doi.org/10.5194/acp-2020-1128
Preprint. Discussion started: 2 December 2020

Understanding the spatiotemporal characteristics of atmospheric CO_2 is a key priority in China because of the central role it plays in regulating the climate and environment. In recent years, tremendous efforts have been made in China to control anthropogenic emissions from fossil fuel combustion for both air quality and climate mitigation purposes (Zheng et al., 2018). While the sources and sinks of air pollutants have been thoroughly examined and well documented (Huang et al., 2020), the dynamics of CO_2 at regional to national scales remain poorly understood due to lack of long-term observations and limited modelling studies (Han et al., 2020). Li et al. (2020) applied a weather-biosphere model with tower observations to analyse CO_2 fluxes and concentrations over mixed forest and rice paddy in northeast China, but the one-year simulation limits the attempt to investigate interannual CO_2 variation which is subject to substantial change (Fu et al., 2019b). Wang et al. (2019) applied satellite products and in-situ observations with inverse modelling to derive posterior carbon fluxes and reported 100% uncertainty for constraining global terrestrial flux. Fu et al. (2020) applied GEOS-Chem simulation with offline Carbon Tracker (Peters et al., 2007) as input to estimate impacts of terrestrial flux and anthropogenic emissions on the annual variation of CO_2 concentrations, but regional-scale assessment was limited by coarse grid resolution (2°×2.5°). Machine-learning technique has also been employed to upscale site observations to regional-scale (Yao et al., 2018; Zhu et al., 2014), but the estimations of carbon budget and dynamics retain large uncertainty due to the diversity of biomass among sites and suffer from coarse grid resolution. These pilot studies have shed light on improving the understanding of spatiotemporal characteristics of CO_2 in China with modelling or observational methods, but an integrated investigation with both modelling and observations at fine-scale is urgently needed to expand diagnostic understanding of localized and regional transport, flux, and concentration of CO_2 to inform emission management and climate adaption policies (Fu et al., 2019a;Niu et al., 2017;Wang et al., 2019).

In this study we apply the Weather Research and Forecasting model coupled with the Vegetation Photosynthesis and Respiration Model (WRF-VPRM) (Hu et al., 2020;Mahadevan et al., 2008) to simulate and characterize the spatiotemporal variation of atmospheric CO_2 in China from 2016-2018, and also to validate this weather-biosphere model with recent advanced satellite and tower observations. WRF-VPRM has been applied in a few case studies over the United States (Hu et al., 2020), Europe (Kretschmer et al., 2012), northeast China (Li et al., 2020), and South Korea (Park et al., 2020); this study is the first attempt to apply and evaluate it for a multi-year simulation at fine scale (20 km) over China. We first describe the modelling methods and data employed followed by model validation against observations from multiple datasets, and then present the spatiotemporal variations and estimates of contributions from anthropogenic emissions, terrestrial flux, and background concentrations. Finally, we probe into tower data and reveal the boundary layer thermal structure impacts on atmospheric CO_2 accumulation and depletion.

2 Method

The WRF-VPRM simulation in this study is configured with 48 vertical layers and 20 km grid resolution. Initial and boundary conditions are derived from the mole fraction product of CarbonTracker (Peters et al., 2007) with 3°×2° resolution. The latest update of column average CO_2 (XCO_2) concentration assimilation product from CarbonTracker (CT2019) with 1°×1°

https://doi.org/10.5194/acp-2020-1128
Preprint. Discussion started: 2 December 2020

resolution is also employed to compare with the WRF-VPRM simulation. The anthropogenic emission inventory is from the Open-source Data Inventory for Anthropogenic CO_2 (ODIAC) with 0.1°×0.1° resolution (Oda et al., 2018) shown in Fig.1(a); ocean flux is from climatology estimation (Takahashi et al., 2009); and vegetation fractions and enhanced vegetation index (EVI, shown in Fig.1(b)) are from MODIS (Huete et al., 2002). CO_2 from initial and boundary conditions, anthropogenic emission, and terrestrial biogenic flux are tagged as BCG, ANT, and BIO, respectively, to allow the contributions from each process to be identified and quantified through one simulation.

WRF-VPRM calculates ecosystem respiration (ER) and gross ecosystem exchange (GEE) with the following functions as:

$$ER = \alpha \times T + \beta \quad (1)$$

$$GEE = -\lambda \times T_{scale} \times W_{scale} \times P_{scale} \times (1 + PAR/PAR_0)^{-1} \times EVI \times PAR \quad (2)$$

where T is the air temperature at 2m above the surface (T2); α, β, λ are vegetation type-dependent parameters; PAR_0 is the vegetation type-dependent half-saturation value of photosynthetically active radiation (PAR); and $T_{scale}, W_{scale}, P_{scale}$ are scaling factors for temperature, water stress, and phenology, respectively. In this study we take the atmosphere as a reference, thus GEE has a negative sign and ER has a positive sign. The current version of WRF-VPRM is parameterized (α, β, λ) for 7 vegetation types (Fig.1(c)): crops, mixed forest, evergreen forest, deciduous forest, shrub, savanna, and grass. For each modelling grid, ER and GEE are calculated as the weighted averages of each vegetation type based on their fractional abundance. Recent studies (Hu et al., 2020;Li et al., 2020) have investigated the uncertainty associated with this parameterization through sensitivity simulations and suggested the crops can be further divided into subcategories based on eddy-covariance (EC) tower measurement to improve the model. In this study we apply the default parameterization, which has been demonstrated to successfully reproduce the terrestrial flux over northeast China (Li et al., 2020). In contrast, CT2019 applies a pure biosphere model, the Carnegie-Ames Stanford Approach (CASA(Zhou et al., 2020)), driven by year-specific weather and satellite data to simulate terrestrial fluxes (Peters et al., 2007). CASA also estimates photosynthetic uptake based on solar radiation and plant phenology, and estimates respiration as a function of T2. CASA directly simulates monthly means of Net Primary Production (NPP) and heterotrophic respiration (R_H). NPP is the difference between photosynthetic uptake (equivalent to GEE) and autotrophic respiration (R_A). The summary of R_H and R_A is equivalent to ER. Thus, WRF-VPRM and CASA are essentially very similar in terms of methodology; however, it should be noted that to resolve CASA simulated NPP into GEE and R_A, CT2019 applies the assumption that GEE is twice that of NPP, which implies that for the same plants the photosynthetic carbon uptake is double the magnitude of autotrophic respiration (but of opposite sign). This assumption is applicable at monthly scale but may contribute to difficulty reproducing the rapid changes at hourly and daily scales due to impact from weather systems, which will be demonstrated with more details in Section 3.2.

Measurements of CO_2 concentrations are collected at the Lin'an Regional Atmospheric Background Station (30.30˚N, 119.75˚E, surroundings shown in Fig.1(d)) with Picarro G1301 and G1302 trace gas analysers mounted on an observation tower at 21 and 55 meters, respectively, above ground level (AGL) and analysed online (data analysis lab shown in Fig.1(e)).

https://doi.org/10.5194/acp-2020-1128
Preprint. Discussion started: 2 December 2020

The station is located in the remote area of Hangzhou 138.6 meters above sea level in the middle of a hilly area covered by mixed forest. The hourly Lin'an station tower measurements collected between 2016-2018 provide a representative sampling of the CO_2 gradients resulting from exchange between atmosphere mixing and terrestrial flux.

Flask samplings of CO_2 surface concentrations with monthly intervals are collected through the National Oceanic and Atmospheric Administration's (NOAA's) Earth System Research Laboratory (ESRL) at four sites (shown in Fig.1(f)) within our modelling domain, including Dongsha Island (DSI, 20.69˚N, 116.73˚E), Lulin (LLN, 23.47˚N, 120.87˚E), Ulaan Uul (UUM, 44.45˚N, 111.09˚E), and Mt. Waliguan (WLG, 36.29˚N, 100.89˚E). The Orbiting Carbon Observatory-2 (OCO-2) satellite product (Kiel et al., 2019) with daily intervals is employed to validate simulation of column averaged CO_2 (XCO_2) concentrations. A total of 204,940 OCO-2 version9 swath data covering the simulation period is used in this study. Daily ground-based Fourier transform spectrometer (FTS) Measured XCO_2 at Hefei site (31.90˚N, 117.17˚E) is also collected through the Total Carbon Column Observing Network (TCCON) for year 2016 (Wang et al., 2017). WRF has been evaluated extensively and consistently performs well for reproducing the meteorology fields and the transport of atmospheric tracers, so this study will present the simulation performance for CO_2 only which hasn't been thoroughly discussed in the literature.

3 Result and Discussion

3.1 Model evaluation

We first evaluate the capability of WRF-VPRM to reproduce concentrations of surface CO_2 and XCO_2, and we find fairly good model performance through the comparison with satellite and ground-based observations. The WRF-VPRM simulated surface layer (mid-level height AGL is 12m) CO_2 and XCO_2 averages between 2016-2018 are demonstrated in Fig.2(a) and (b) respectively. High concentrations are found over industrial areas such as the North China Plain (NCP), Pearl River Delta (PRD), and Yangtze River Delta (YRD), where the surface CO_2 and XCO_2 are above 440 ppmv and 408 ppmv, respectively; the domain averages are 411 ppmv and 406 ppmv, respectively. While most climate models assume evenly distributed CO_2 (Fung et al., 1983;Kiehl and Ramanathan, 1983), our data demonstrates a prominent gradient between industrial and remote areas (e.g., Tibet Plateau, Mongolia), especially for surface CO_2, which could be an important source of uncertainty for estimating the long-wave radiation effect (Xie et al., 2018). Spatial patterns of CO_2 and XCO_2 are in close agreement with ODIAC, indicating the dominant impact of anthropogenic emission in determining the CO_2 distribution. WRF-VPRM simulated CO_2 is generally consistent with CT2019 (Fig.2(d)), but CT2019 estimates lower surface CO_2 (mid-level height AGL is 25m) over the coastal industrial areas YRD and PRD because the ocean module used in CT2019 estimates stronger air-sea exchange than the ocean flux by Takahashi et al. (2009) used in WRF-VPRM. The two models show better agreement for XCO_2 (Fig.2(e)), but also differ by ~1 ppmv over Taklamakan Desert and along the eastern side of the Tibet Plateau. The OCO-2 swath data are integrated into the corresponding horizontal grids of WRF-VPRM and CT2019, respectively, to validate XCO_2. Biases of WRF-VPRM and CT2019 both fall into the range of ±3 ppmv as shown in Fig.2(d) and (f), respectively, but

https://doi.org/10.5194/acp-2020-1128
Preprint. Discussion started: 2 December 2020

WRF-VPRM apparently provides more details of spatial gradient. WRF-VPRM shows well-mixed underestimations and overestimations along neighbouring satellite tracks, while CT2019 tends to overestimate (underestimate) over Tibet Plateau (Taklamakan Desert) where WRF-VPRM gives slightly smaller biases. In general, the WRF-VPRM model reproduces OCO-2 well, with mean bias (MB) of 0.76 ppmv and normalized mean bias (NMB) of 0.19% (Fig.3(a)); CT2019 shows MB of 0.54 ppmv and NMB of 0.17% (Fig.3(b)), suggesting an overall acceptable performance of the weather-biosphere model to reproduce the spatial distribution pattern of XCO_2 in China.

We further analyse WRF-VPRM validation against OCO-2 for the seven vegetation types in each season and find no prominent difference (evaluation statistics summarized in Table 1). Regarding vegetation type, the model shows the largest normalized mean bias (NMB) of -0.25% and 0.31% in summer and winter, respectively, both over deciduous forest which only covers a very small portion in northeast China (see dominant vegetation types in Fig.1(c)). The three most abundant coverage vegetation types in China are grass, crops, and mixed forest. XCO_2 simulated by WRF-VPRM over grass areas is slightly overestimated by 0.08~0.16% throughout the year, and the NMB over mixed forest is -0.11%~0.15%, indicating a good performance of the model over the vast majority of areas of China. Performance over crops generally shows larger discrepancy than other vegetation types, with NMB ranging from 0.16% in summer to 0.29% in winter, suggesting the model tends to slightly overestimate column concentration of CO_2 over cropland. Li et al. (2020) reported that WRF-VPRM underestimated biosphere carbon over rice paddy sites (by ~3%) in northeast China and suggested the parameterization of α, β, λ as the most important cause. Cropland differs significantly across China with various types of species such as rice, wheat, and corn, for which literature reports substantially different rates of ecosystem respiration and photolysis uptake (Gao et al., 2018;Yang et al., 2016;Zhu et al., 2020). Thus, applying one set of parameters to represent all crops may be responsible for the lingering uncertainty of simulated XCO_2. In terms of seasonal difference, WRF-VRPM performs best in summer (NMB=0.12%) and worst in winter (NMB=0.23%), and the correlation coefficients are all ~0.8, consistent with application over the U.S. (Hu et al., 2020) which also reported slightly better performance in summer than other seasons, indicating good agreement with the OCO-2 satellite product.

Fig.3 presents the overall simulation bias against observations employed in this study at the raw temporal intervals (daily for OCO-2, daily for TCCON at Hefei, hourly for tower data at Lin'an, and monthly for data at ESRL sites). Surface CO_2 concentrations are simulated well with minor overestimation by 0.69 ppmv (0.17%) at the ESRL sites (Fig.3(f)). However, evaluation at the Lin'an station shows significant overestimations for CO_2 by 5.34 ppmv (1.25%) and 5.41 ppmv (1.27%) at 21m (Fig.3(d)) and 55m (Fig.3(e)) AGL, respectively; the mid-level heights of WRF-VPRM's first, second, and third layers are 12.3m, 36.9m, and 61.6m, respectively, and simulations are linearly interpolated to compare with the tower data. The discrepancy is largely attributable to the vertical allocation of anthropogenic emission within the model as recently recognized (Brunner et al., 2019). Biosphere models (such as WRF-VPRM and CASA) and inverse modelling methods allocate anthropogenic CO_2 emission into the surface layer due to lack of injection height information, which will likely lead to systematic overestimation of surface CO_2 concentration in industrial areas; though a regional scale (750×650km) modelling

https://doi.org/10.5194/acp-2020-1128
Preprint. Discussion started: 2 December 2020

study around the city of Berlin (Brunner et al., 2019) reported that distributing anthropogenic emission into the surface layer overestimated near-surface CO_2 concentration by 14% in summer and 43% in winter as compared with considering the vertical profiles of local anthropogenic sources. CT2019 also substantially overestimates at Lin'an, but the first, second, and third layers' mid-level heights are 25m, 103m, and 247m, respectively, so we did not compare it directly with the tower data, but analysed the simulated diurnal variation as will be discussed in Section 3.3. Fig.3(c) and (d) reveal that observed average CO_2 concentrations at Lin'an (428 ppmv) are substantially higher than those at ESRL sites (407-410 ppmv). The evaluation at Lin'an station also infers the prominent high CO_2 level in YRD due to the intensive regional anthropogenic emission as compared with ESRL sites at remote locations. Pu et al. (Pu et al., 2014) analysed the back trajectories for hourly measurements collected at Lin'an station between 2009-2011 and demonstrated that it was frequently affected by prevailing northeast winds carrying polluted airmasses from upwind cities including Hangzhou, Shanghai, and northeast parts of Jiangsu where manufacturing factories were densely located. Simulated XCO_2 is also compared with TCCON Hefei site observations, and a very good agreement is found with MB of -0.79 ppmv and NMB of -0.2%. In general, recent atmospheric inverse modelling studies (Fu et al., 2019a;Wang et al., 2019;Xie et al., 2018) report the simulation bias of XCO_2 as 0.5-2 ppmv with posterior flux inputs. The WRF-VPRM model has demonstrated good agreement with the observations as a process-based model though our evaluation.

3.2 CO_2 seasonal variation and trend in China

We next analyse the seasonality of CO_2 and XCO_2 and find that the terrestrial flux plays a more influential role than anthropogenic emission. WRF-VPRM successfully reproduces seasonal variations of CO_2 at ESRL sites, with a correlation coefficient of 0.90 (Fig.4(a)), but the correlation between simulated and observed CO_2 at Lin'an tower is only 0.67 (Fig.4(c)); we will probe into bias at Lin'an in the next section. Both the model and measurements show prominent seasonal cycles for surface CO_2 concentrations, with maximums in April (413-419 ppmv) and minimums in August (399-404 ppmv) as shown in Fig.4(b). The model suggests that the anthropogenic CO_2 contribution is 2.6 ppmv in both months, while the biogenic contributions are 3.1 ppmv and -1.2 ppmv in April and August, respectively (Fig.4(d)). Anthropogenic emission (Fig.4(f)) shows a flat curve with relatively higher values in December due to fuel combustion for heating (Zheng et al., 2018); EVI meanwhile shows maximums in July and August (Fig.4(f)). During summer, photosynthetic uptake almost completely offsets anthropogenic emission, causing the minimum CO_2 concentration observed in August, while the higher anthropogenic emission in December and respiration flux in April lead to the two corresponding peaks. The anthropogenic XCO_2 contributions from are 0.5 and 0.6 ppmv in April and August, respectively, and the biogenic contributions are 0.8 ppmv and -1.5 ppmv, respectively, suggesting that the seasonality of XCO_2 is also primarily dominated by terrestrial flux. Furthermore, the seasonality at high-latitude ESRL sites (UUM and WLG) is stronger than at Lin'an and low-latitude sites (DSI and LLN) because of the larger temperature and photosynthetically active radiation (PAR) gradients. Annual average anthropogenic and biogenic XCO_2 contributions are 7.1 ppmv and -1.9 ppmv, respectively, indicating that biosphere uptake is an important carbon sink offsetting 27% of anthropogenic emission and slowing the growth of atmospheric CO_2.

https://doi.org/10.5194/acp-2020-1128
Preprint. Discussion started: 2 December 2020

Atmospheric Chemistry and Physics Discussions

XCO_2 shows similar seasonality, with minimums in August and maximums in April and December (Fig.4(b)). Both WRF-VPRM and CT2019 show good agreement with TCCON Hefei observations with correlations of 0.89 and 0.88, respectively (Fig.4(e)). However, we note that WRF-VPRM simulates drastic changes (e.g., the grey shaded period in Fig.4(e)) that are not shown by CT2019; Fig. 5 shows the daily concentrations of XCO_2 overlaid with horizontal wind speed at 10m AGL from WRF-VPRM and CT2019 and highlights large discrepancies over Hefei. Between April 1st and 3rd 2016, an 850 hPa trough associated with a surface cold front moved southeastward from Mongolia to the North China Plain (NCP) (weather maps shown in Fig.5(g)-(i)). At the leading edge of the front, a convergence zone associated with a low pressure center formed, which led to significant cloud formation and subsequently reduced short-wave radiation. As a result, photosynthetic carbon uptake was reduced, leading to enhancement of atmospheric CO_2. Meanwhile, the cold front transported anthropogenic CO_2 from NCP to YRD, and the convergence zone along YRD ahead of the front facilitated the accumulation of air pollutants and CO_2 from anthropogenic emissions. With its coarse spatiotemporal resolution, CT2019 has difficulty reproducing such regional weather systems that can lead to rapid and localized changes in CO_2 concentration and terrestrial flux, indicating the importance of fine resolution modelling to better represent the small spatial scale and rapid temporal scale variations of CO_2 (Agusti-Panareda et al., 2019).

We also find a notable increasing trend for the 3-year study period. Observed CO_2 annual enhancement is 0.56%/yr (2.2 ppmv/yr) at the ESRL sites and 0.67%/yr (2.8 ppmv/yr) at Lin'an. The slightly higher growth rate at Lin'an can be attributed to the influence of the regional anthropogenic emission, which is growing at rate of 0.82%/yr as suggested by ODIAC. Domain-wide XCO_2 is also found to increase by 0.57%/yr (2.3 ppmv/yr) as suggested by OCO-2 and 0.61%/yr (2.5 ppmv/yr) as suggested by the simulation. WRF-VPRM reproduces the trends in good agreement with ground and satellite observations. Model simulated budgets suggests that the increasing trends for anthropogenic, biogenic, and background XCO_2 are 0.81%/yr, -9.17%/yr, and 0.59%/yr, respectively; the trends for anthropogenic, biogenic, and background CO_2 are 4.95%/yr, -0.73%/yr, and 0.59%/yr, respectively. Our findings are consistent with recent measurements and inverse modelling studies but provide process-based estimates for anthropogenic emission and terrestrial flux. Wu et al. (Wu et al., 2012) reported measured CO_2 concentration at Changbai Mountain forest site in northeast China increased by 1.76 ppmv/yr between 2003-2010. With the atmospheric inversion modelling method, Fu et al. (2019b) estimated surface CO_2 in East Asia increased by 2-3 ppmv/yr between 2004-2012. These trends suggest that although anthropogenic emission increased at a steady rate in East Asia, photosynthetic uptake also served as an increasing carbon sink due to enhanced EVI (0.29%/yr). However, as the interannual variability (IAV) of terrestrial flux is usually critically large and is affected by both vegetation itself and climate conditions (Fu et al., 2019b;Niu et al., 2017), simulation over longer time periods is necessary to conclusively comment on the changing trend of biosphere CO_2 in China.

https://doi.org/10.5194/acp-2020-1128
Preprint. Discussion started: 2 December 2020

3.3 Diurnal variation of near-surface CO_2 and influence factors

Finally, we examine the diurnal variation of meteorology and CO_2 data at Lin'an station as shown in Fig.6 to reveal the temporal dynamics and atmospheric mixing of CO_2 at local scale. While both 21m and 55m CO_2 show prominent diurnal changes, the variations are larger in summer (JJA) than winter (DJF) and are larger at 21m than 55m, indicating the dominant influence of terrestrial flux over anthropogenic emission in determining the near surface CO_2 concentration. Fig.6(c) presents the diurnal change of wind speed collected at 50m of the Lin'an tower. The higher wind speed between 10:00-22:00 local time suggests strong regional transport and mixing of CO_2 mainly occurs during this period. Fig.6(d) and (g) present the WRF-VPRM and CT2019 simulation bias, respectively, against Lin'an tower data at 21m (note the Y-scales are different). We find that both models prominently overestimate during night time. Li et al. (2020) reported the model overestimated NEE at a mixed forest site Wuying by 34% during the growing season (May-Sep.) according to EC measurement. Fig.6(f) and (i) present the simulated NEE by WRF-VPRM and CT2019, respectively, which show close correlations with the CO_2 simulation biases. While Lin'an is also covered by mixed forest, our evaluation suggests that WRF-VPRM may have also estimated nighttime ecosystem respiration during the non-growing season, and CT2019 has even greater bias for presenting the diurnal cycles of terrestrial flux.

We also find that planetary boundary layer height (PBLH) significantly affects diurnal accumulation and depletion of atmospheric CO_2 as shown in Fig.7(a). During daytime in the growing season, photosynthetic uptake results in lower CO_2 concentration; meanwhile, PBLH is also high and allows rapid vertical mixing between near surface and upper air. During nighttime when photosynthesis stops, CO_2 from ecosystem respiration starts to accumulate in the shallow stable boundary layer, while the residual layer remains largely decoupled. Thus, atmospheric constituents with surface sources normally exhibit a vertical profile in which concentrations decrease with height in the stable boundary layer (Hu et al., 2020;Hu et al., 2012). Such boundary layer characteristics are confirmed by CO_2 vertical gradients at Lin'an. CO_2 at 55m height is consistently lower than the near surface air at 21m during nighttime due to accumulation of respired CO_2 in the stable boundary layer. As photosynthetic uptake depletes the near surface CO_2 and daytime boundary layer convection develops, the CO_2 gradient is gradually weakened from 06:00 to 11:00 LT and remains minimal through the rest of the daytime; at midday when photosynthesis reaches maximum intensity, CO_2 at 21m is even lower than at 55m. WRF-VPRM generally reproduces the diurnal profile but noticeably underestimates the intensity of night time ΔCO_2, likely due to the bias for simulating night time terrestrial flux as discussed above or underestimation of nighttime boundary layer stability by the PBL scheme (Hu et al., 2012).

The relationship between the near-surface CO_2 profile and boundary layer stability is further statistically examined. Fig.7(b) presents the correlation between air temperature gradient ($\Delta T/\Delta H$) and CO_2 concentration gradient ($\Delta CO_2/\Delta H$) calculated with annual averaged diurnal tower observations, which clearly demonstrates the influence of boundary layer stability on the CO_2 vertical profile. On one hand, a more stable PBL with a strongly positive temperature gradient would promote surface CO_2 accumulation and lead to a strongly negative CO_2 gradient, especially under inversion conditions when upper air has higher temperature (orange area in Fig.7(b)). Conversely, a strongly negative temperature gradient indicates stronger radiation, and subsequently greater photosynthesis and CO_2 depletion in the near surface layer, which would result in a positive CO_2 gradient (green area in Fig.7(b)) implying a lower CO_2 concentration at the surface. While the diurnal variations of ΔCO_2 are primarily dictated by local biogenic CO_2 fluxes and boundary layer dynamics, the two minor daytime peaks of ΔCO_2 at Lin'an, at 10:00 and 18:00 LT (Fig.7(a)) likely suggest influence of transport of CO_2 from urban plumes in the region; for example, from Hangzhou which is 60 km away from the tower. Due to rush-hours anthropogenic emissions, CO_2 enhancement at Hangzhou relative to a background site exhibits a prominent bimodal curve with two peaks during early morning and early evening (Pu et al., 2018). Depending on meteorological conditions, particularly wind fields, urban CO_2 plumes from cities such as Hangzhou may be transported to the Lin'an site. Due to higher altitude and stronger winds – wind profile increases with height at Lin'an according to observations (figure not shown) – 55m at the Lin'an tower has a larger footprint than 21m, thus 55m on the tower is more likely affected by the urban plumes in the region than 21m. The 10:00 and 18:00 LT ΔCO_2 peaks at Lin'an likely suggest stronger CO_2 enhancement at 55 m than at 21m from influence of regional anthropogenic emissions; the slight delay of these ΔCO_2 peaks relative to rush hours (at about 08:00 and 17:00 LT) further corroborate the hypothesis of delayed influence of transport of urban CO_2 from Hangzhou. Even though 55m has a larger footprint than at 21m and thus may be more likely affected by regional urban emissions, turbulent vertical mixing may reduce the different influence from regional urban emissions, which explains the fact that ΔCO_2 peaks are only minor. The influence of boundary layer conditions on CO_2 variability has been discussed in several studies through analysis of mountain site ground-based observations (Arrillaga et al., 2019;Esteki et al., 2017;Li et al., 2014), but our study applies tower data as direct evidence to demonstrate the significant impact of PBL thermal structure, which has rarely been documented. More importantly, although WRF-VPRM fails to capture the bimodal ΔCO_2 peaks at rush hours, because monthly ODIAC data lacks an hourly profile, our analysis reveals the critical importance of careful configuration of the PBL scheme and spatiotemporal distribution of anthropogenic emission for weather-biosphere modelling of atmospheric CO_2.

4 Summary and Conclusions

In this study, the spatiotemporal variations of CO_2 in China are investigated with measurements from multiple datasets and a weather-biosphere coupled model simulation for 2016-2018. We find consistent higher concentrations over industrial areas with excessive anthropogenic emission and lower concentrations over densely vegetated areas. Observed CO_2 concentrations at Lin'an (427 ppmv) are significantly higher than remote ESRL sites (408 ppmv) although they are all established as "background" stations, indicating the dominant influence of anthropogenic emission at regional scales. The Lin'an tower data shows a large negative correlation (-0.85) between vertical CO_2 concentration and air temperature gradients, suggesting the significant influence of boundary layer stability on CO_2 accumulation and depletion. The online coupled weather-biosphere model WRF-VPRM enables process-based estimations of contributions from anthropogenic emission (0.59 ppmv (0.15%)), terrestrial flux (0.16 ppmv (-0.04%)), and background concentration (405.70 ppmv (99.89%)) to average total XCO_2.

https://doi.org/10.5194/acp-2020-1128
Preprint. Discussion started: 2 December 2020

Respective simulation biases of surface CO_2 and XCO_2 are 0.69 ppmv (0.17%) and 0.76 ppmv (0.19) against ESRL site observations and OCO-2 satellite product with correlations of 0.87 and 0.90, indicating overall good performance of the WRV-VPRM model. Maximum CO_2 concentrations are found in April and minimums are found in August for all three years, and the seasonality is reproduced well by the model, which also reveals that terrestrial flux and background concentration dominated the seasonality rather than anthropogenic emission.

A steadily increasing trend in XCO_2 by ~0.6%/yr during the study period is demonstrated consistently by both model simulation and satellite product. Budget analysis suggests that anthropogenic emission increased by 0.83%/yr contributing to the 0.81%/yr growth rate of anthropogenic XCO_2 enhancement, 27% of which was offset by biosphere uptake. It is noted that terrestrial flux has significant inter-annual variability, thus a more robust estimation of the terrestrial flux trend should be obtained through a long-term study in the future. The background XCO_2, representing contributions from global circulation, increased by 0.59%/yr, suggesting that CO_2 level in China was growing at the same rate as the rest of the world.

The most significant modelling bias is identified from validation against the Lin'an tower data, which WRF-VPRM overestimated by about 5.38 ppmv (1.26%) with a correlation coefficient of 0.67. The allocation of anthropogenic emission into the surface layer is partially responsible for this modelling bias because Lin'an is closely affected by upwind industrial mega cities in YRD, suggesting the need to include vertical profiles of fossil fuel combustion to properly redistribute the ODIAC for modelling purposes. However, diurnal variations of the bias suggest that the modelling discrepancy is likely due to large uncertainty associated with simulating ecosystem respiration during the nighttime. Representation and parameterization of photosynthetic carbon uptake in VPRM has been continuously improved during the past 10 years since its first release (Hu et al., 2020), but ecosystem respiration parameterization is still too simplified to fully represent the autotrophic and heterotrophic respiration of biomass. Nevertheless, WRF-VPRM is demonstrated to be a reliable tool to model the dynamics of CO_2 and exchange between the atmosphere and terrestrial flux. Most importantly, as the online coupled modelling system is able to simulate meteorology and biosphere processes simultaneously, it promotes the opportunity to investigate the interactions between atmospheric mixing and terrestrial flux (Carvalhais et al., 2014;Schimel et al., 2015) while comprehensively considering various factors from both sides that affect CO_2 in one coordinate frame, which could be a very helpful tool to support policy makers for balancing short-term carbon cycles at regional scales.

Data availability

The modelling output is accessible by contacting the corresponding author (yjjiang@pku.org.cn, xhu@ou.edu)

Author contributions

The concept and ideas to design the integrated simulation and observation analysis were devised by YJ, X-MH, and XD. Simulation was performed by X-MH. OCO-2 satellite product was collected and processed by X-MH. CT2019 assimilation data and ground-based observations were collected by XD. Tower measurement was conducted, processed, and analysed by

https://doi.org/10.5194/acp-2020-1128
Preprint. Discussion started: 2 December 2020

Atmospheric Chemistry and Physics Discussions

QM, JP, and YJ. Model evaluation was performed by MY. The manuscript was prepared by XD and X-MH with input and feedback from YJ, MY, QM, JP, and GZ.

Competing interests

The authors declare that they have no conflict of interest.

Acknowledgements

This work is supported by the Fundamental Research Funds for the Central Universities (14380049) and National Key Research and Development Program of China (2016YFC0201900). We thank NASA and NOAA ESRL for providing the public accessible satellite products and observations used in this study. OCO-2 data was collected through https://co2.jpl.nasa.gov/#mission=OCO-2. ESRL surface flask CO_2 data was downloaded from https://www.esrl.noaa.gov/gmd/dv/data.html. TCCON data was downloaded from https://data.caltech.edu/records/1092. CarbonTracker data was downloaded from https://www.esrl.noaa.gov/gmd/ccgg/carbontracker/download.php.

https://doi.org/10.5194/acp-2020-1128
Preprint. Discussion started: 2 December 2020

Atmospheric Chemistry and Physics
Discussions

References

Agusti-Panareda, A., Diamantakis, M., Massart, S., Chevallier, F., Munoz-Sabater, J., Barre, J., Curcoll, R., Engelen, R., Langerock, B., Law, R. M., Loh, Z., Morgui, J. A., Parrington, M., Pench, V. H., Ramonet, M., Roehl, C., Vermeulen, A. T., Warneke, T., and Wunch, D.: Modelling CO2 weather - why horizontal resolution matters, Atmos Chem Phys, 19, 7347-7376, 2019.

Ahmadov, R., Gerbig, C., Kretschmer, R., Koerner, S., Neininger, B., Dolman, A. J., and Sarrat, C.: Mesoscale covariance of transport and CO2 fluxes: Evidence from observations and simulations using the WRF-VPRM coupled atmosphere-biosphere model, J Geophys Res-Atmos, 112, 2007.

Ahmadov, R., Gerbig, C., Kretschmer, R., Korner, S., Rodenbeck, C., Bousquet, P., and Ramonet, M.: Comparing high resolution WRF-VPRM simulations and two global CO2 transport models with coastal tower measurements of CO2, Biogeosciences, 6, 807-817, 2009.

Arrillaga, J. A., Yague, C., Roman-Cascon, C., Sastre, M., Jimenez, M. A., Maqueda, G., and de Arellano, J. V. G.: From weak to intense downslope winds: origin, interaction with boundary-layer turbulence and impact on CO2 variability, Atmos Chem Phys, 19, 4615-4635, 2019.

Brunner, D., Kuhlmann, G., Marshal, J., Clement, V., Fuhrer, O., Broquet, G., Loscher, A., and Meijer, Y.: Accounting for the vertical distribution of emissions in atmospheric CO2 simulations, Atmos Chem Phys, 19, 4541-4559, 2019.

Carvalhais, N., Forkel, M., Khomik, M., Bellarby, J., Jung, M., Migliavacca, M., Mu, M. Q., Saatchi, S., Santoro, M., Thurner, M., Weber, U., Ahrens, B., Beer, C., Cescatti, A., Randerson, J. T., and Reichstein, M.: Global covariation of carbon turnover times with climate in terrestrial ecosystems, Nature, 514, 213-+, 2014.

Crowell, S. M. R., Kawa, S. R., Browell, E. V., Hammerling, D. M., Moore, B., Schaefer, K., and Doney, S. C.: On the Ability of Space-Based Passive and Active Remote Sensing Observations of CO2 to Detect Flux Perturbations to the Carbon Cycle, J Geophys Res-Atmos, 123, 1460-1477, 2018.

Dayalu, A., Munger, J. W., Wofsy, S. C., Wang, Y. X., Nehrkorn, T., Zhao, Y., McElroy, M. B., Nielsen, C. P., and Luus, K.: Assessing biotic contributions to CO2 fluxes in northern China using the Vegetation, Photosynthesis and Respiration Model (VPRM-CHINA) and observations from 2005 to 2009, Biogeosciences, 15, 6713-6729, 2018.

Esteki, K., Prakash, N., Li, Y. L., Mu, C., and Du, K.: Seasonal Variation of CO2 Vertical Distribution in the Atmospheric Boundary Layer and Impact of Meteorological Parameters, Int J Environ Res, 11, 707-721, 2017.

Feng, S., Lauvaux, T., Keller, K., Davis, K. J., Rayner, P., Oda, T., and Gurney, K. R.: A Road Map for Improving the Treatment of Uncertainties in High-Resolution Regional Carbon Flux Inverse Estimates, Geophys Res Lett, 46, 13461-13469, 2019.

Fu, Y., Liao, H., Tian, X. J., Gao, H., Cai, Z. N., and Han, R.: Sensitivity of the simulated CO2 concentration to inter-annual variations of its sources and sinks over East Asia, Adv Clim Chang Res, 10, 250-263, 2019a.

Fu, Z., Stoy, P. C., Poulter, B., Gerken, T., Zhang, Z., Wakbulcho, G., and Niu, S. L.: Maximum carbon uptake rate dominates the interannual variability of global net ecosystem exchange, Global Change Biol, 25, 3381-3394, 2019b.

Fung, I., Prentice, K., Matthews, E., Lerner, J., and Russell, G.: 3-Dimensional Tracer Model Study of Atmospheric Co2 - Response to Seasonal Exchanges with the Terrestrial Biosphere, J Geophys Res-Oceans, 88, 1281-1294, 1983.

Gao, Y. Q., Lee, X. H., Liu, S. D., Hu, N., Hu, C., Liu, C., Zhang, Z., and Yang, Y. C.: Spatiotemporal variability of the near-surface CO2 concentration across an industrial-urban-rural transect, Nanjing, China, Sci Total Environ, 631-632, 1192-1200, 2018.

Gaubert, B., Stephens, B. B., Basu, S., Chevallier, F., Deng, F., Kort, E. A., Patra, P. K., Peters, W., Rodenbeck, C., Saeki, T., Schimel, D., Van der Laan-Luijkx, I., Wofsy, S., and Yin, Y.: Global atmospheric CO2 inverse models converging on neutral tropical land exchange, but disagreeing on fossil fuel and atmospheric growth rate, Biogeosciences, 16, 117-134, 2019.

Han, P. F., Zeng, N., Yao, B., Zhou, W. J., Chen, L. Q., Wang, S. Q., Lv, H. G., Xiao, W., Zhu, L. Y., and Xu, J. P.: Preface to Special Topic on Atmospheric Greenhouse Gas Measurement and Application in China, Adv Atmos Sci, 37, 555-556, 2020.

Hu, X. M., Doughty, D. C., Sanchez, K. J., Joseph, E., and Fuentes, J. D.: Ozone variability in the atmospheric boundary layer in Maryland and its implications for vertical transport model, Atmos Environ, 46, 354-364, 2012.

Hu, X. M., Crowell, S., Wang, Q. Y., Zhang, Y., Davis, K. J., Xue, M., Xiao, X. M., Moore, B., Wu, X. C., Choi, Y., and DiGangi, J. P.: Dynamical Downscaling of CO2 in 2016 Over the Contiguous United States Using WRF-VPRM, a Weather-Biosphere-Online-Coupled Model, Jounal of Advances in Modeling Earth Systems, 12, 10.1029/2019MS001875, 2020.

https://doi.org/10.5194/acp-2020-1128
Preprint. Discussion started: 2 December 2020

Huang, X., Ding, A. J., Wang, Z. L., Ding, K., Gao, J., Chai, F. H., and Fu, C. B.: Amplified transboundary transport of haze by aerosol-boundary layer interaction in China, Nat Geosci, 13, 428-+, 2020.

Huete, A., Didan, K., Miura, T., Rodriguez, E. P., Gao, X., and Ferreira, L. G.: Overview of the radiometric and biophysical performance of the MODIS vegetation indices, Remote Sens Environ, 83, 195-213, 2002.

Kiehl, J. T., and Ramanathan, V.: Co2 Radiative Parameterization Used in Climate Models - Comparison with Narrow-Band Models and with Laboratory Data, J Geophys Res-Oceans, 88, 5191-5202, 1983.

Kiel, M., O'Dell, C. W., Fisher, B., Eldering, A., Nassar, R., MacDonald, C. G., and Wennberg, P. O.: How bias correction goes wrong: measurement of X-CO2 affected by erroneous surface pressure estimates, Atmos Meas Tech, 12, 2241-2259, 2019.

Kondo, M., Patra, P. K., Sitch, S., Friedlingstein, P., Poulter, B., Chevallier, F., Ciais, P., Canadell, J. G., Bastos, A., Lauerwald, R., Calle, L., Ichii, K., Anthoni, P., Arneth, A., Haverd, V., Jain, A. K., Kato, E., Kautz, M., Law, R. M., Lienert, S., Lombardozzi, D., Maki, T., Nakamura, T., Peylin, P., Rodenbeck, C., Zhuravlev, R., Saeki, T., Tian, H. Q., Zhu, D., and Ziehn, T.: State of the science in reconciling top-down and bottom-up approaches for terrestrial CO2 budget, Global Change Biol, 26, 1068-1084, 2020.

Kretschmer, R., Gerbig, C., Karstens, U., and Koch, F. T.: Error characterization of CO2 vertical mixing in the atmospheric transport model WRF-VPRM, Atmos Chem Phys, 12, 2441-2458, 2012.

Li, X. L., Hu, X. M., Cai, C. J., Jia, Q. Y., Zhang, Y., Liu, J. M., Xue, M., Xu, J. M., Wen, R. H., and Crowell, S. M. R.: Terrestrial CO2 Fluxes, Concentrations, Sources and Budget in Northeast China: Observational and Modeling Studies, J Geophys Res-Atmos, 125, 2020.

Li, Y., Deng, J., Mu, C., Xing, Z., and Du, K.: Vertical distribution of CO2 in the atmospheric boundary layer: Characteristics and impact of meteorological variables, Atmos Environ, 91, 110-117, 2014.

Mahadevan, P., Wofsy, S. C., Matross, D. M., Xiao, X. M., Dunn, A. L., Lin, J. C., Gerbig, C., Munger, J. W., Chow, V. Y., and Gottlieb, E. W.: A satellite-based biosphere parameterization for net ecosystem CO2 exchange: Vegetation Photosynthesis and Respiration Model (VPRM), Global Biogeochem Cy, 22, 2008.

Niu, S. L., Fu, Z., Luo, Y. Q., Stoy, P. C., Keenan, T. F., Poulter, B., Zhang, L. M., Piao, S. L., Zhou, X. H., Zheng, H., Han, J. Y., Wang, Q. F., and Yu, G. R.: Interannual variability of ecosystem carbon exchange: From observation to prediction, Global Ecol Biogeogr, 26, 1225-1237, 2017.

Oda, T., Maksyutov, S., and Andres, R. J.: The Open-source Data Inventory for Anthropogenic CO2, version 2016 (ODIAC2016): a global monthly fossil fuel CO2 gridded emissions data product for tracer transport simulations and surface flux inversions, Earth Syst Sci Data, 10, 87-107, 2018.

Papale, D., and Valentini, A.: A new assessment of European forests carbon exchanges by eddy fluxes and artificial neural network spatialization, Global Change Biol, 9, 525-535, 2003.

Park, C., Gerbig, C., Newman, S., Ahmadov, R., Feng, S., Gurney, K. R., Carmichael, G. R., Park, S. Y., Lee, H. W., Goulden, M., Stutz, J., Peischl, J., and Ryerson, T.: CO2 Transport, Variability, and Budget over the Southern California Air Basin Using the High-Resolution WRF-VPRM Model during the CalNex 2010 Campaign, J Appl Meteorol Clim, 57, 1337-1352, 2018.

Park, C., Park, S. Y., Gurney, K. R., Gerbig, C., DiGangi, J. P., Choi, Y., and Lee, H. W.: Numerical simulation of atmospheric CO2 concentration and flux over the Korean Peninsula using WRF-VPRM model during Korus-AQ 2016 campaign, Plos One, 15, 2020.

Peters, W., Jacobson, A. R., Sweeney, C., Andrews, A. E., Conway, T. J., Masarie, K., Miller, J. B., Bruhwiler, L. M. P., Petron, G., Hirsch, A. I., Worthy, D. E. J., van der Werf, G. R., Randerson, J. T., Wennberg, P. O., Krol, M. C., and Tans, P. P.: An atmospheric perspective on North American carbon dioxide exchange: CarbonTracker, P Natl Acad Sci USA, 104, 18925-18930, 10.1073/pnas.0708986104, 2007.

Peylin, P., Baker, D., Sarmiento, J., Ciais, P., and Bousquet, P.: Influence of transport uncertainty on annual mean and seasonal inversions of atmospheric CO2 data, J Geophys Res-Atmos, 107, 2002.

Peylin, P., Law, R. M., Gurney, K. R., Chevallier, F., Jacobson, A. R., Maki, T., Niwa, Y., Patra, P. K., Peters, W., Rayner, P. J., Rodenbeck, C., van der Laan-Luijkx, I. T., and Zhang, X.: Global atmospheric carbon budget: results from an ensemble of atmospheric CO2 inversions, Biogeosciences, 10, 6699-6720, 2013.

Pu, J. J., Xu, H. H., He, J., Fang, S. X., and Zhou, L. X.: Estimation of regional background concentration of CO2 at Lin'an Station in Yangtze River Delta, China, Atmos Environ, 94, 402-408, 2014.

Pu, J. J., Hu, H. H., Jiang, Y. J., Du, R. G., and Qi, B.: Characteristics of and factors affecting atmospheric CO2 concentration in Hangzhou, Environmental Science, 39, 10.13227/j.hjkx.201708258, 2018.

Schimel, D., Stephens, B. B., and Fisher, J. B.: Effect of increasing CO2 on the terrestrial carbon cycle, P Natl Acad Sci USA, 112, 436-441, 2015.

Shi, Z., Crowell, S., Luo, Y. Q., and Moore, B.: Model structures amplify uncertainty in predicted soil carbon responses to climate change, Nat Commun, 9, 2018.

Takahashi, T., Sutherland, S. C., Wanninkhof, R., Sweeney, C., Feely, R. A., Chipman, D. W., Hales, B., Friederich, G., Chavez, F., Sabine, C., Watson, A., Bakker, D. C. E., Schuster, U., Metzl, N., Yoshikawa-Inoue, H., Ishii, M., Midorikawa, T., Nojiri, Y., Kortzinger, A., Steinhoff, T., Hoppema, M., Olafsson, J., Arnarson, T. S., Tilbrook, B., Johannessen, T., Olsen, A., Bellerby, R., Wong, C. S., Delille, B., Bates, N. R., and de Baar, H. J. W.: Climatological mean and decadal change in surface ocean pCO(2), and net sea-air CO2 flux over the global oceans (vol 56, pg 554, 2009), Deep-Sea Res Pt I, 56, 2075-2076, 2009.

Tian, H. Q., Lu, C. Q., Yang, J., Banger, K., Huntzinger, D. N., Schwalm, C. R., Michalak, A. M., Cook, R., Ciais, P., Hayes, D., Huang, M. Y., Ito, A., Jain, A. K., Lei, H. M., Mao, J. F., Pan, S. F., Post, W. M., Peng, S. S., Poulter, B., Ren, W., Ricciuto, D., Schaefer, K., Shi, X. Y., Tao, B., Wang, W. L., Wei, Y. X., Yang, Q. C., Zhang, B. W., and Zeng, N.: Global patterns and controls of soil organic carbon dynamics as simulated by multiple terrestrial biosphere models: Current status and future directions, Global Biogeochem Cy, 29, 775-792, 2015.

Todd-Brown, K. E. O., Randerson, J. T., Post, W. M., Hoffman, F. M., Tarnocai, C., Schuur, E. A. G., and Allison, S. D.: Causes of variation in soil carbon simulations from CMIP5 Earth system models and comparison with observations, Biogeosciences, 10, 1717-1736, 2013.

Wang, H. M., Jiang, F., Wang, J., Ju, W. M., and Chen, J. M.: Terrestrial ecosystem carbon flux estimated using GOSAT and OCO-2 XCO2 retrievals, Atmos Chem Phys, 19, 12067-12082, 2019.

Wang, W., Tian, Y., Liu, C., Sun, Y. W., Liu, W. Q., Xie, P. H., Liu, J. G., Xu, J., Morino, I., Velazco, V. A., Griffith, D. T., Notholt, J., and Warneke, T.: Investigating the performance of a greenhouse gas observatory in Hefei, China, Atmos Meas Tech, 10, 2627-2643, 2017.

Wu, J. B., Guan, D. X., Yuan, F. H., Yang, H., Wang, A. Z., and Jin, C. J.: Evolution of atmospheric carbon dioxide concentration at different temporal scales recorded in a tall forest, Atmos Environ, 61, 9-14, 2012.

Xie, X. D., Huang, X. X., Wang, T. J., Li, M. M., Li, S., and Chen, P. L.: Simulation of Non-Homogeneous CO2 and Its Impact on Regional Temperature in East Asia, J Meteorol Res-Prc, 32, 456-468, 2018.

Yang, S. H., Xu, J. Z., Liu, X. Y., Zhang, J. G., and Wang, Y. J.: Variations of carbon dioxide exchange in paddy field ecosystem under water-saving irrigation in Southeast China, Agr Water Manage, 166, 42-52, 2016.

Zheng, B., Tong, D., Li, M., Liu, F., Hong, C. P., Geng, G. N., Li, H. Y., Li, X., Peng, L. Q., Qi, J., Yan, L., Zhang, Y. X., Zhao, H. Y., Zheng, Y. X., He, K. B., and Zhang, Q.: Trends in China's anthropogenic emissions since 2010 as the consequence of clean air actions, Atmos Chem Phys, 18, 14095-14111, 2018.

Zhou, Y., Williams, C. A., Lauvaux, T., Davis, K. J., Feng, S., Baker, I., Denning, S., and Wei, Y.: A Multiyear Gridded Data Ensemble of Surface Biogenic Carbon Fluxes for North America: Evaluation and Analysis of Results, Journal of Geophysical Research: Biogeosciences, 125, e2019JG005314, 10.1029/2019jg005314, 2020.

Zhu, Z. L., Tang, X. Z., and Zhao, F. H.: Comparison of Ozone Fluxes over a Maize Field Measured with Gradient Methods and the Eddy Covariance Technique, Adv Atmos Sci, 37, 586-596, 2020.

https://doi.org/10.5194/acp-2020-1128
Preprint. Discussion started: 2 December 2020

Table 1. Evaluation statistics[1] for WRF-VPRM against OCO-2 satellite product at daily intervals

Season	Vegetation type	Mean Obs. (ppmv)	Mean Sim. (ppmv)	MB[2] (ppmv)	NMB[2] (%)	cc[2]	# of samples
Spring	other	406.85	407.81	0.96	0.23[1]	0.82	16123
	evergreen	407.52	407.89	0.36	0.09	0.73	1920
	deciduous	408.15	408.430	0.27	**0.07**[1]	0.82	412
	mixed	407.79	408.21	0.41	0.10	0.79	4438
	shrubland	406.97	407.54	0.56	0.13	0.74	6550
	savanna	407.59	408.55	0.96	0.22	0.81	534
	grass	406.81	407.49	0.68	0.16	0.81	11170
	crops	407.50	408.29	0.79	0.19	0.82	13548
Summer	other	403.90	404.84	0.93	0.23	0.88	13445
	evergreen	402.68	402.24	-0.44	-0.11	0.85	1082
	deciduous	400.39	399.39	-1.01	-0.25	0.82	527
	mixed	402.04	401.60	-0.43	-0.11	0.87	4312
	shrubland	403.92	404.41	0.48	0.12	0.85	5193
	savanna	404.62	404.60	-0.02	**0.01**	0.79	170
	grass	402.35	402.66	0.31	0.08	0.88	12588
	crops	402.86	403.52	0.66	0.16	0.87	7947
Fall	other	403.32	404.35	1.03	0.26	0.82	17054
	evergreen	403.93	403.19	-0.74	-0.18	0.71	1716
	deciduous	403.35	403.64	0.28	**0.07**	0.84	281
	mixed	403.64	403.95	0.31	0.08	0.83	3611
	shrubland	403.12	404.22	1.10	0.27	0.77	8532
	savanna	403.45	404.15	0.70	0.17	0.70	504
	grass	403.22	403.65	0.43	0.11	0.85	11176
	crops	403.76	404.80	1.04	0.26	0.80	13136
Winter	other	404.76	405.80	1.03	0.26	0.80	13838
	evergreen	404.79	404.75	-0.05	**-0.01**	0.78	2671
	deciduous	405.38	406.65	1.27	0.31	0.79	135
	mixed	405.20	405.79	0.59	0.15	0.79	2108
	shrubland	404.76	405.84	1.09	0.27	0.79	7683
	savanna	404.63	405.83	1.20	0.30	0.75	1064
	grass	405.06	405.64	0.58	0.14	0.77	5967
	crops	405.17	406.36	1.19	0.29	0.79	15508

[1]For each season, evaluation statistic with the worst performance (largest absolute value of NMB) is highlighted in red, and the one with best performance (smallest absolute value of NMB) is highlighted with in bold font.

[2] $MB = \frac{1}{N}\sum_{i=1}^{N}(Sim_i - Obs_i)$, $NMB = \frac{\sum_{i=1}^{N}(Sim_i - Obs_i)}{\sum_{i=1}^{N} Obs_i}$, $cc = \frac{\sum_{i=1}^{N}(Sim_i - \bar{S}im)(Obs_i - \bar{O}bs)}{\sqrt{\sum_{i=1}^{N}(Sim_i - \bar{S}im)^2}\sqrt{\sum_{i=1}^{N}(Obs_i - \bar{O}bs)^2}}$, where $\bar{S}im$ is the average of simulations, $\bar{O}bs$ is the average of observations.

https://doi.org/10.5194/acp-2020-1128
Preprint. Discussion started: 2 December 2020

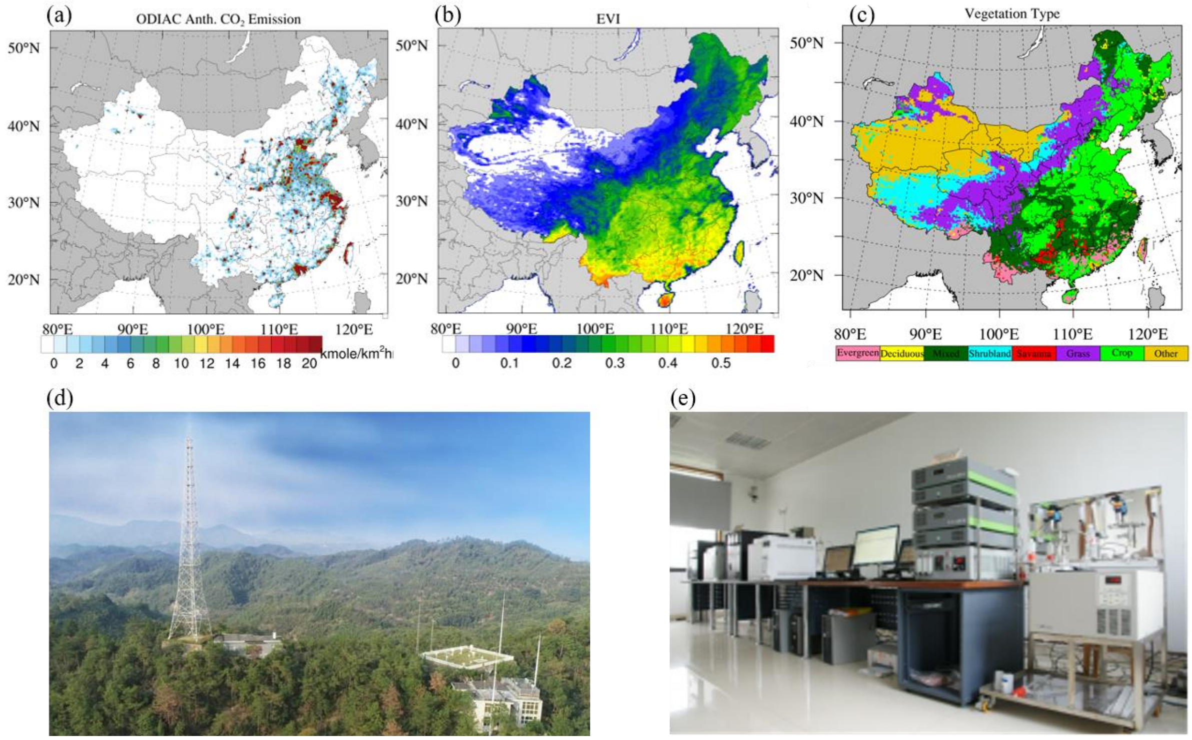

Figure 1: Annual averages of (a) ODIAC emission, (b) MODIS EVI, and (c) dominant vegetation type; and (d) photo of Lin'an observation tower; (e) photo of data analysis and recording system

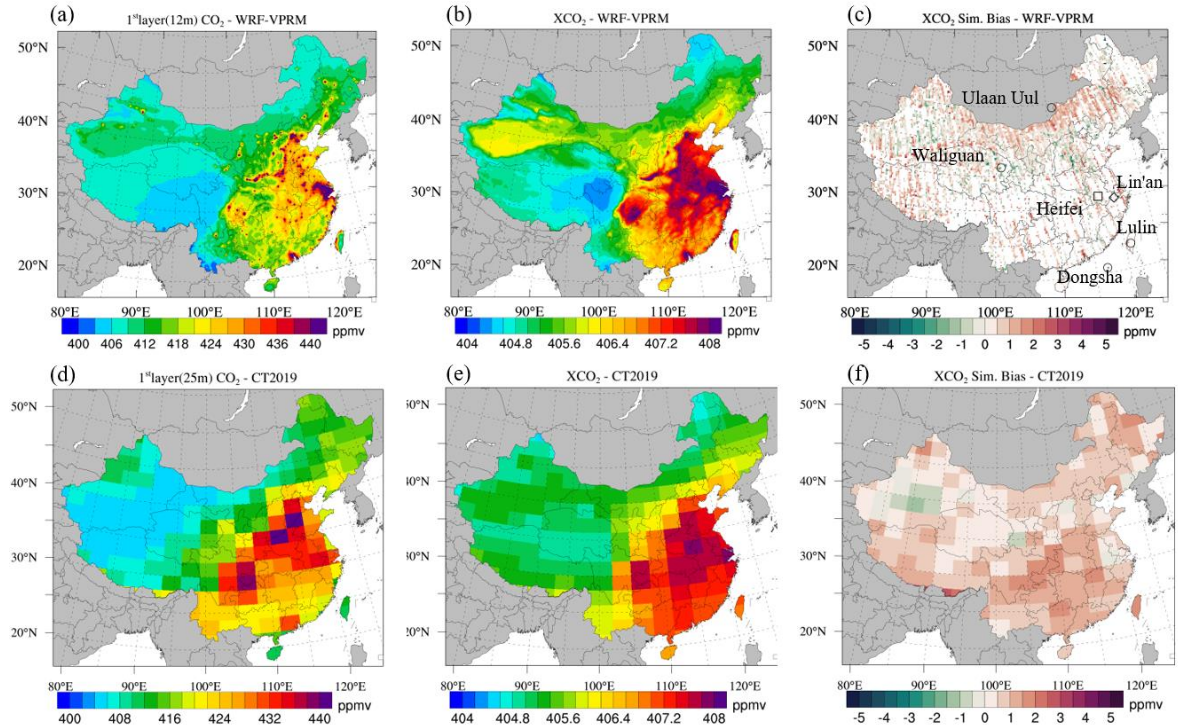

Figure 2: 2016-2018 averages of WRF-VPRM simulations of (a) 1st layer (mid-layer height is 12km) CO_2 concentration, and (b) XCO_2 concentration; (c) WRF-VPRM simulated XCO_2 bias against OCO-2; (d)-(f) is same as (a)-(c) but for CT2019 (1st layer mid-level height is 25m). Markers in (c) represent the locations of ground-based sites.

https://doi.org/10.5194/acp-2020-1128
Preprint. Discussion started: 2 December 2020

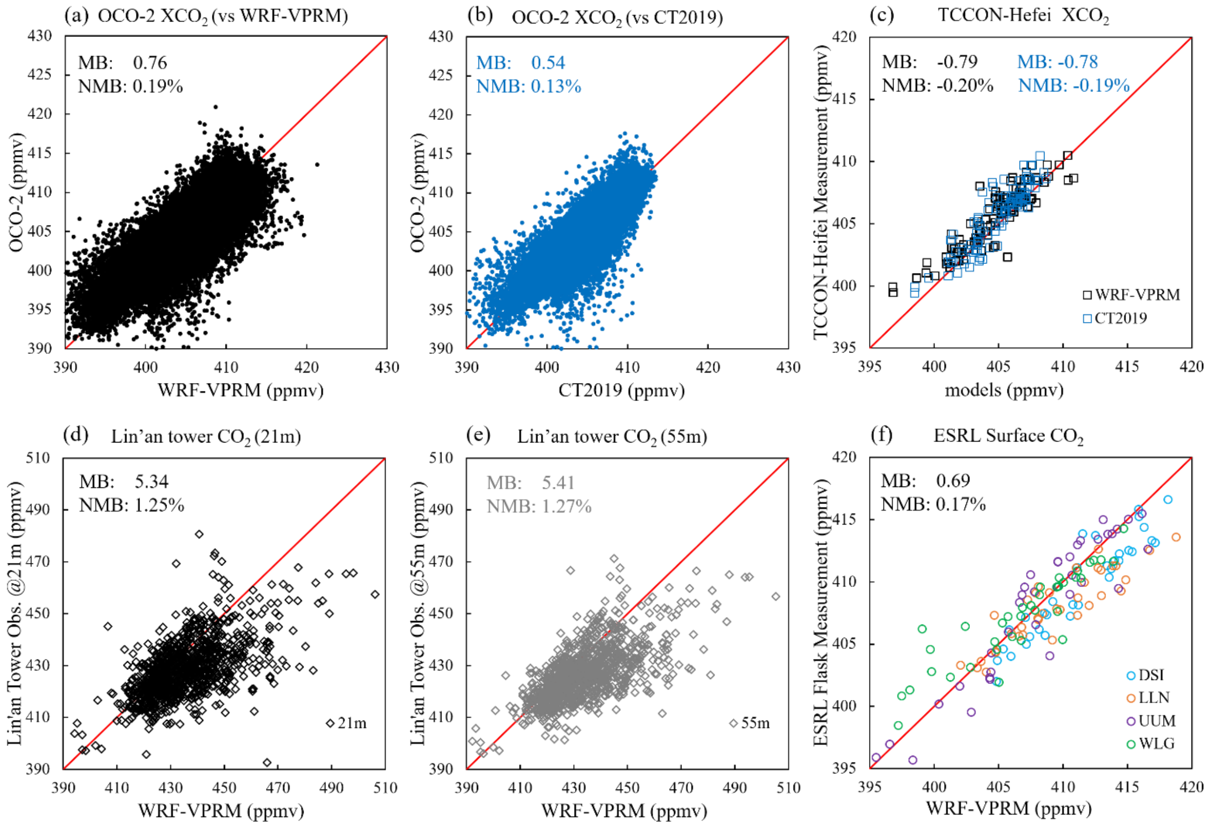

Figure 3: Data pairs for OCO-2 against (a) WRF-VPRM and (b) CT2019, (c) TCCON-Hefei against WRF-VPRM and CT2019, Lin'an tower against WRF-VPRM at (d) 21m and (e) 55m, and (f) ESRL against WRF-VPRM

https://doi.org/10.5194/acp-2020-1128
Preprint. Discussion started: 2 December 2020

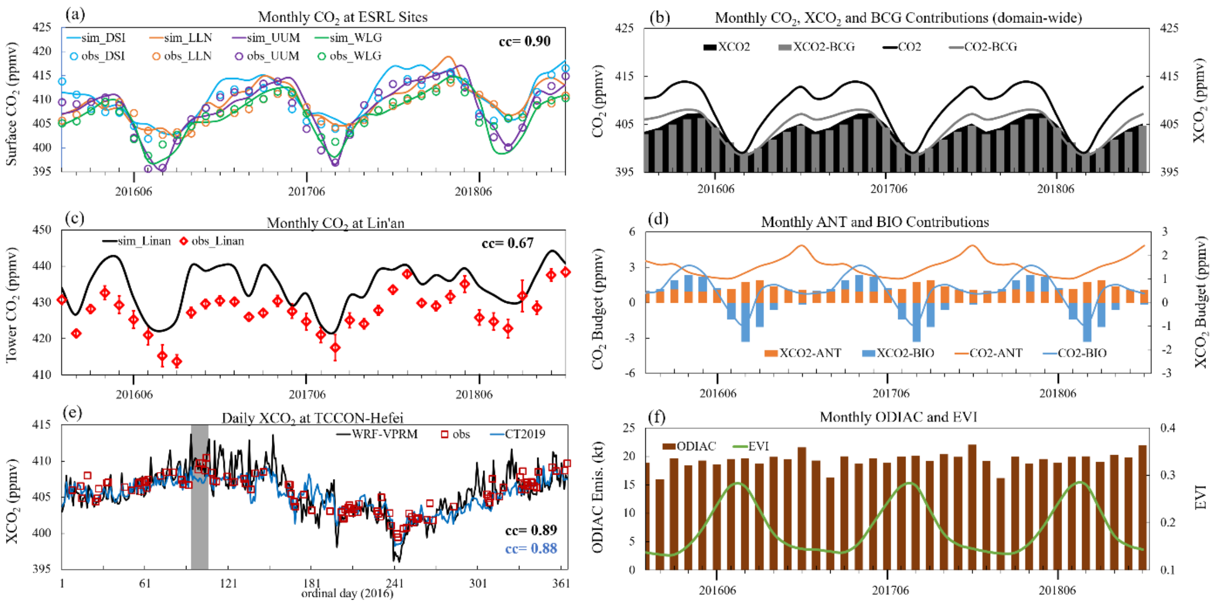

Figure 4: Monthly variations of (a) CO_2 at ESRL sites, (b) total (black) and background (BCG, grey) CO_2 (line) and XCO_2 (area and bar), (c) CO_2 at Lin'an station (averaged for 21m and 55m data); (d) contributions from anthropogenic (ANT, orange) and biogenic (BIO, blue) for CO_2 (lines) and XCO_2 (bars); (f) ODIAC emission and MODIS EVI; and (e) Daily variation of XCO_2 at TCCON-Hefei site

https://doi.org/10.5194/acp-2020-1128
Preprint. Discussion started: 2 December 2020

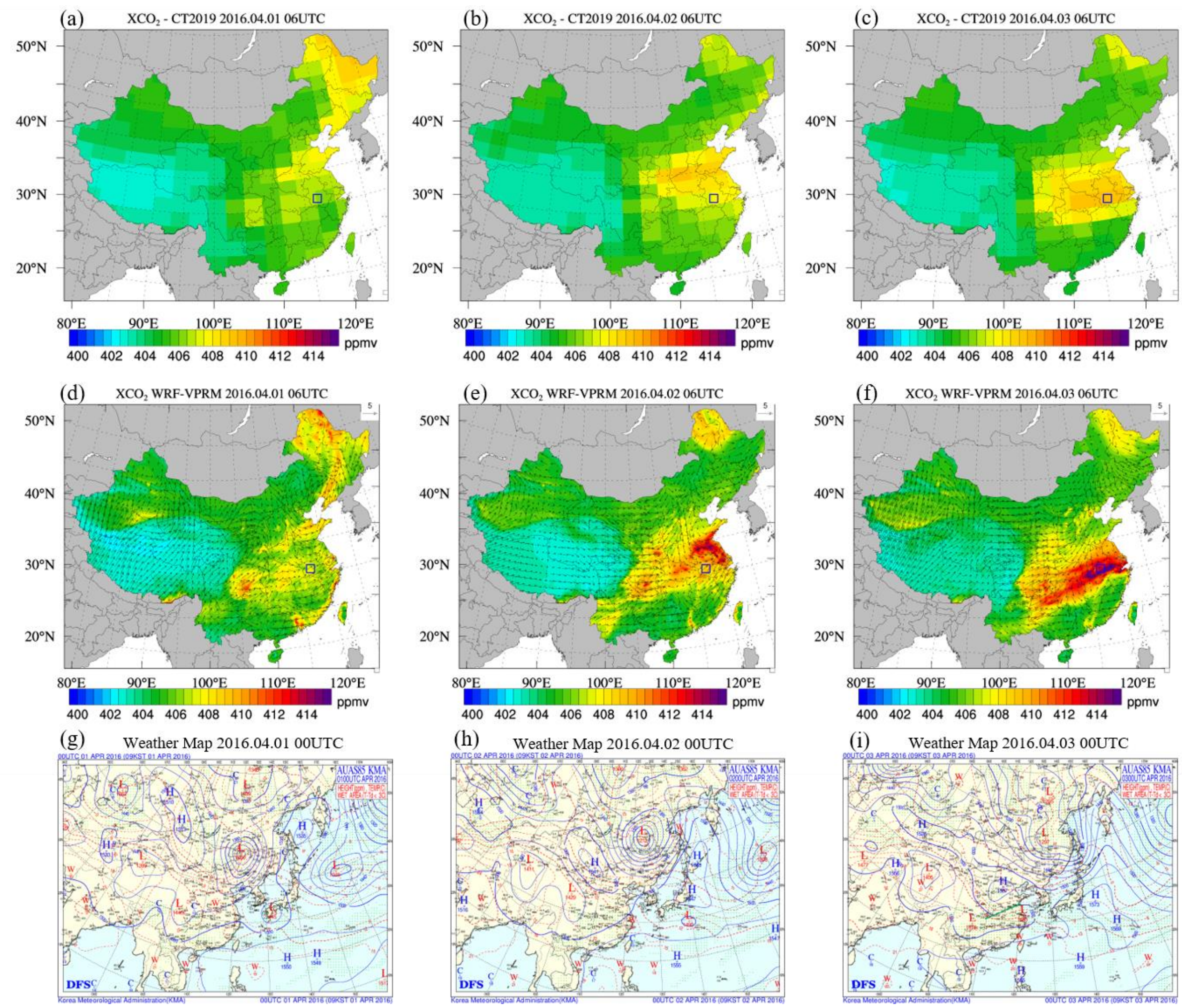

Figure 5: Daily XCO_2 from CT2019 (a-c) and WRF-VPRM (d-f), weather map from Korea Meteorological Administration (g-i). The blue box represents location of Hefei.

535

https://doi.org/10.5194/acp-2020-1128
Preprint. Discussion started: 2 December 2020

Atmospheric Chemistry and Physics
Discussions
Open Access
EGU

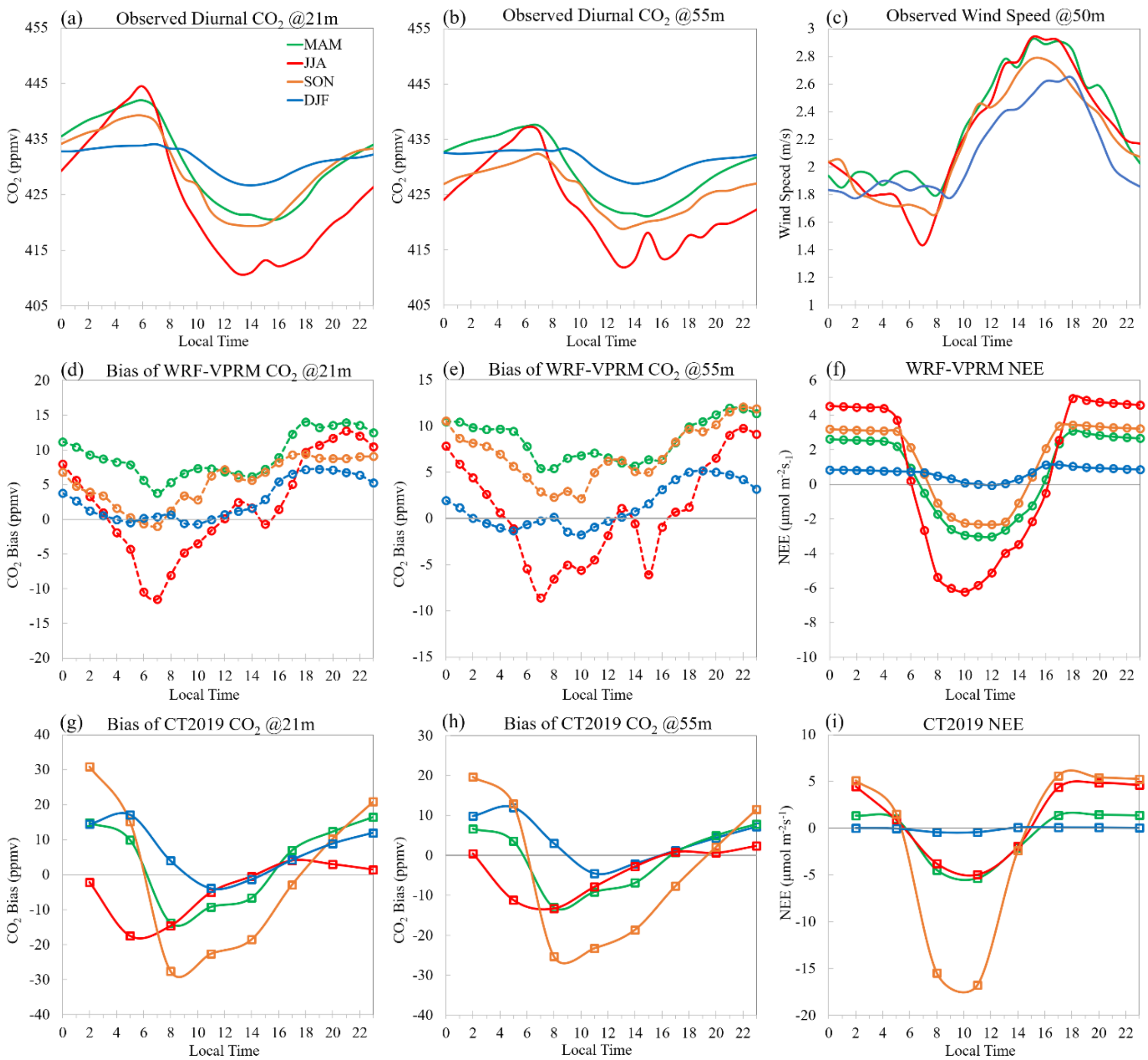

Figure 6: Seasonal mean diurnal variations of observed CO_2 at (a) 21m and (b) 55m, and (c) wind speed at 50m; WRF-VPRM simulation biases of CO_2 at (d) 21m and (e) 55m, and (f) simulated NEE; (g)-(i) are same as (d)-(f) but for CT2019.

https://doi.org/10.5194/acp-2020-1128
Preprint. Discussion started: 2 December 2020

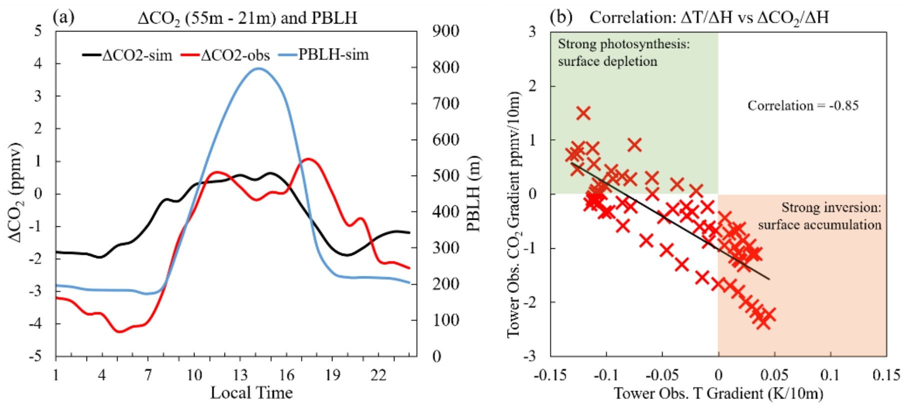

Figure 7: (a) Average (2016-2018) diurnal variations of simulated (black line) and observed (red line) ΔCO_2 and simulated (blue line) PBLH at Lin'an station; and (b) correlation between CO_2 gradient between 55m and 21m ($\Delta CO_2/\Delta H$) and temperature gradient ($\Delta T/\Delta H$) at Lin'an station (diurnal data is averaged for each year respectively).